"Virtual Fragment Linking": An Approach To Identify Potent Binders from Low Affinity Fragment Hits

Thomas J. Crisman,[†] Andreas Bender,[†] Mariusz Milik,[†] Jeremy L. Jenkins,[†] Josef Scheiber,[†] Sai Chetan K. Sukuru,[†] Jasna Fejzo,[†] Ulrich Hommel,[‡] John W. Davies,[†] and Meir Glick*[,†]

Center for Proteomic Chemistry, Novartis Institutes for BioMedical Research, Inc., 250 Massachusetts Avenue, Cambridge, Massachusetts 02139, and Center for Proteomic Chemistry, Novartis Pharma AG, Postfach, CH-4002 Basel, Switzerland

Received October 18, 2007

In this work we explore the possibilities of using fragment-based screening data to prioritize compounds from a full HTS library, a method we call virtual fragment linking (VFL). The ability of VFL to identify compounds of nanomolar potency based on micromolar fragment binding data was tested on 75 target classes from the WOMBAT database and succeeded in 57 cases. Further, the method was demonstrated for seven drug targets from in-house screening programs that performed both FBS of 8800 fragments and screens of the full library. VFL captured between 28% and 67% of the hits ($IC_{50} < 10\mu M$) in the top 5% of the ranked library for four of the targets (enrichment between 5-fold and 13-fold). Our findings lead us to conclude that proper coverage of chemical space by the fragment library is crucial for the VFL methodology to be successful in prioritizing HTS libraries from fragment-based screening data.

1. Introduction

High-throughput screening (HTS[a]) is a hit-finding technique frequently used in pharmaceutical industry that attempts to discover compounds active against a particular target by screening large libraries (by "brute force").[1] A state of the art HTS platform contains about 1−5 million compounds that could be screened in a few weeks. Despite this impressive throughput, there is a constant pressure to reduce the costs associated with HTS and maximize the return on investment. Apart from the financial challenge, screening collections capture only a fraction of chemical space where estimates for the total number of organic molecules are in the range of 10^{18}–10^{200} compounds.[2,3] Therefore, chemical space of typical drug-sized molecules is not sampled sufficiently. It is estimated that the screening collections of all pharmaceutical companies collectively target only around 1000 proteins.[4] This has led to the oversampling of certain areas of chemical space, in particular those compounds synthesized around "hot" targets like metabolic enzymes, GPCRs, and more recently, kinases. This focus on target classes of "current interest" created a fundamental lack of broad diversity in most pharmaceutical screening collections while at the same time enriching local diversity in particular regions of chemical space.

An alternative avenue that has emerged over the past few years to help address the escalating costs and the limited chemical novelty is fragment based screening (FBS).[5–7] By screening a small library that contains hundreds to thousands of low molecular weight (MW < 300 Da) and structurally simple fragments, one can more efficiently sample chemical space.[8] Because of the inherent low affinity of the fragments that are typically in the millimolar range, it is difficult to measure the IC_{50} values in a traditional bioassay. In those cases alternative methods have been developed to obtain a reliable signal that include biophysical screening using X-ray crystallography[9] and NMR.[10]

Starting from a fragment binding with millimolar activity in the binding pocket, various approaches exist to extend the fragment into a full fledged ligand of the target of interest.[6,10,11] Fragments can be "grown" by exploring the binding potential of neighboring groups by varying appendices of the initial fragment. Alternatives are linking two fragments known to be binders, since a union of fragments binds much more tightly than its constituent parts because of favorable entropy gains in the case of an appropriate linker. Still, exploration of the correct linker consumes experimental time and effort. Under the right circumstances fragment self-assembly might be used, with reactive groups "automatically" assembling fragments in the right places. Regardless of the screening method, developing low affinity fragment hits into a lead by fragment evolution, fragment linking, or fragment self-assembly is challenging.

In this work, we describe a novel computational approach we term "virtual fragment linking" (VFL) that attempts to bridge the gap from fragment to ligand. It generates statistical models based on fragments found in fragment-based screenings (which are active in the milli- to micromolar range) and makes predictions about a full HTS library in order to discover compounds active in the nanomolar range. Its novelty lies in the fact that training data are fragment-based screening data (with MW < 250), while predictions are made for typical HTS small molecules (with MW > 250). Thereby we hoped to be able to use smaller-scale fragment based screening in order to (1) determine what type of small molecules will be active on the target (develop a hypothesis) and (2) prioritize our HTS library and screening only selected compounds from it (execute a focused screening strategy).

2. Methods

(a) "Virtual Fragment Linking" (VFL) Method. "Virtual fragment linking" comprises the statistical analysis of fragment-based screening data (with associated milli- to micromolar

* To whom correspondence should be addressed. Phone: +1-617-871-7130. Fax: +1-617-871-4088. E-mail: meir.glick@novartis.com.
[†] Novartis Institutes for BioMedical Research, Inc.
[‡] Novartis Pharma AG.

[a] Abbreviations: ERβ, estrogen receptor β; ECFPs, extended connectivity fingerprints; FBS, fragment based screening; HTS, high-throughput screening; iNOS, inducible nitric oxide synthase; NO, nitric oxide; ROC, receiver operating characteristic; VFL, virtual fragment linking; WOMBAT, World of Molecular Bioactivity database.

10.1021/jm701314u CCC: $40.75
Published on Web 03/22/2008

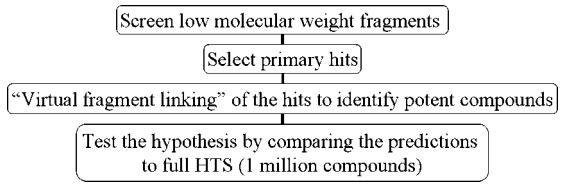

Figure 1. Workflow of the main analyses performed in this work for both the WOMBAT and the in-house data sets. These are the collection of data from fragment-based screening campaigns (low molecular weight binders). Activity models are generated on active fragments via "virtual fragment linking". These activity models are finally used to prioritize compounds from the full HTS set.

activities) in order to make predictions about the activities of the full set of HTS compounds (with associated nanomolar or even better activities). This flowchart is illustrated in Figure 1. The core idea is that by using suitable mathematical modeling procedures, in our case Bayes models, we are able to generalize from the activity of two or more separate fragments in the fragment-based screening to the activity of a molecule in the full HTS library showing both (or more) of those fragments. In the current work we will initially apply VFL to 75 activity classes from WOMBAT to gain statistical insight into the model performance, followed by an analysis of in-house data that leads us to a discussion of details of the model behavior.

We can illustrate VFL through an example taken from the WOMBAT database for inducible nitric oxide synthase (iNOS). This enzyme is responsible for the synthesis of nitric oxide (NO) from the terminal nitrogen atom of L-arginine in the presence of NADPH and oxygen (O_2). Overexpression of iNOS is associated with inflammatory diseases such as rheumatoid arthritis; therefore, down-regulation of iNOS could be of immense value for a rheumatoid arthritis therapy.[12]

We start out with information about the fragment-based screening data on this set. For this data set the IC_{50} and molecular weight distribution for the training set as well as the test set are shown in the upper left corner of Figure 2. We can see that the training (i.e., fragment) set consists of ligands binding at micromolar value and at a molecular weight below 250. On the other hand, the test (i.e., HTS) set shows larger molecules with MW > 250 and IC_{50} values in the nanomolar range. Some of the fragments found active are depicted in the top part of Figure 3. In this example, IC_{50} values of 1.1–32.0 μM are reported for the fragments. On the basis of this set of active fragments, extended connectivity fingerprints (ECFPs) with a radius of 4 were calculated as descriptors upon which our fragment-based activity models are trained. ECFPs were selected as chemical descriptors because they contain attachment points that are essential when linking the fragments into compounds with a higher molecular weight.[13] Further, it has been established that statistical models built using circular fingerprints work well with noisy data such as HTS[14] and that they capture more information than other current molecular descriptors based on their respective performance in a retrospective virtual screening study on a standard benchmark data set.[13,15,16] For this reason we are confident in our choice of ECFPs descriptors for the study performed here.

In this regard it is essential to distinguish between *fragments*, which represent physical low molecular weight compounds used in fragment-based screening, and ECFPs *features*, which represent substructures of the fragments. Thus, a (physical) *fragment* is composed of a set of *features*. Those features are represented in the center part of Figure 3, and they contain information about the local environment of a heavy atom, as well as possibly a set of attachment points. Figure 3 shows 15 samples features out of the hundreds of features contained in the active fragments. For example, aryl ethers, pyridines, piperidine-*N*-esters, and chlorobenzyl functions can be readily identified among the statistically significant features, as well as the set of active fragments depicted above (from which the features were derived).

A Laplacian-modified naive Bayesian classification model as implemented in the SciTegic Pipeline Pilot 6.0 package[17] is then trained on the basis of the features in the data set. The derivation of the Laplacian-modified Bayesian model has been described previously.[18,19] The overall probability ($P_{combined}$) for a compound having activity for a particular target is determined by the product of individual feature frequencies in the data set. In the example above, aryl ethers and pyridines are common in the active fragment data set; therefore, hypothetical new molecules containing those fragments have a high probability of being active against iNOS.

In the last stage the Bayesian model is applied on a collection of compounds with higher molecular weight. It then identifies compounds with a favorable score that we would assume to be active, based on the fragment-based screening data. A selection of molecules we predict as being active (which indeed are actives) are depicted in the lower part of Figure 3. As can be seen, pyridines and piperidine-*N*-esters are among the active molecules, in agreement with our fragment-based screening data. (We are only showing part of the fragments, features, and potent compounds in the figure that would otherwise allow for many more mappings to be found.) The statistically significantly features for the biological activity the model captured in potent iNOS inhibitors are highlighted in red. In this particular case, the aminopyridine derivatives (**1** and **2**) were described by Connolly et al.[12] as selective iNOS inhibitors. Both compounds are potent, with IC_{50} values in the double-digit nanomolar range and so are more active than the fragments we used to train the model. In agreement with experimental results, the 2-methylaminopyridine and 4-piperidine groups were identified by VFL as a desirable features. The 4-piperidine carbamate portion that confers selectivity in compound **2** was captured as well. In compounds **3** and **4** described by Tinker et al.,[20] VFL successfully captured the spirocyclic scaffold.

Overall, we can see that the prediction of active compounds more potent than the training set by several orders of magnitude can be achieved. We will analyze the performance of our model in a more quantitative manner in the Results and Discussion.

(b) WOMBAT Data Sets. We employ two data sets to examine how well one can predict HTS actives from fragment-based screening data. The World of Molecular Bioactivity (WOMBAT)[21] database was used to benchmark the method on a wide variety of different data sets. WOMBAT 2006.1 contains 154 236 entries (136 091 unique SMILES) with biological activity on 1320 unique targets. This comprises 6801 different series from 6791 different papers published in medicinal chemistry journals between 1975 and 2005. Target classes that contained fragments were selected for this study, namely, low molecular weight compounds (<250 Da) with low potency (double- or single-digit micromolar IC_{50} values). In the case of selection of fragments from the WOMBAT database, biochemical assays were used for binding detection. Overall, 75 targets with 14 714 compounds and fragments were identified and selected for this study. The targets along with the sizes of the data sets and the performance data for each model discussed later in this work are given in Table 1.

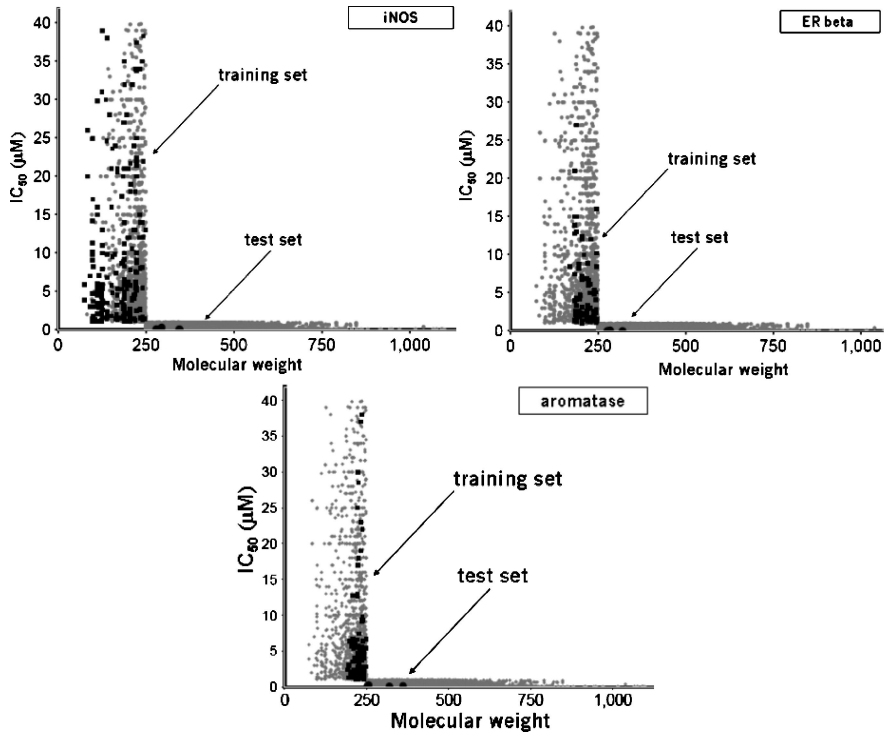

Figure 2. Molecular weight (*X*-axis) versus IC_{50} (*Y*-axis) for the WOMBAT data set. The test and training sets for three activity classes iNOS, ER β, and aromatase are in black. The remainder of the data set is in gray. The weak actives with low molecular weight ("fragment-like") were used as a training set to predict the highly potent compounds for the same activity class.

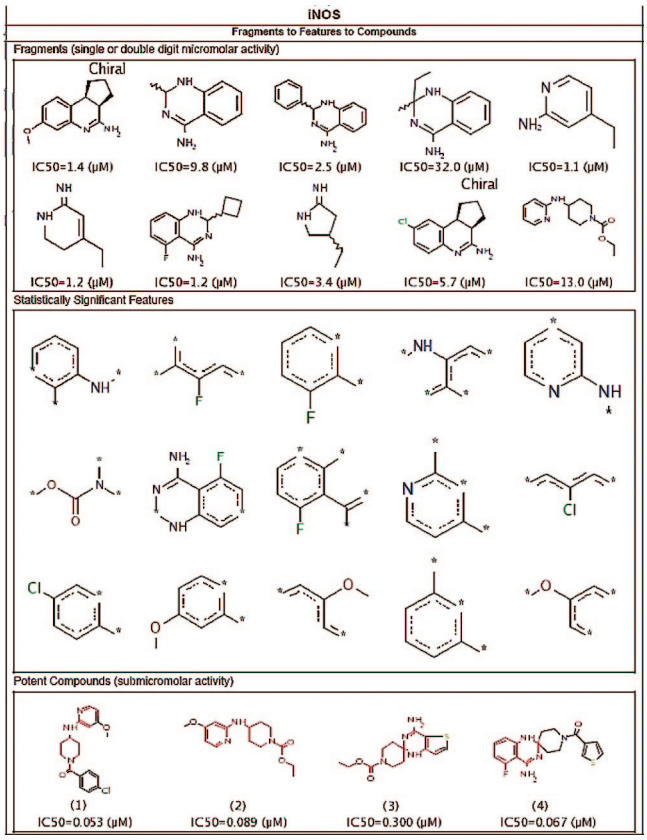

Figure 3. Analysis of the fragments active against iNOS, features contained within the fragments, and HTS compounds that contain features previously found in the fragment set (marked in red).

(c) In-House FBS Data Sets. The Novartis in-house fragment library contains 8800 fragments, and it formed the second data set on which we evaluated virtual fragment linking. We compiled FBS as well as HTS screening data from both biochemical and cell-based assays against the same set of seven targets. These targets include three kinases, a GPCR, an estrogen receptor, a metalloproteinase, and an ion channel as detailed in Table 2. The fragments selected for the library either were purchased from external vendors based on molecular weight and solubility values or were synthesized in-house through lead optimization projects and exploratory chemistry. The fragments were screened at one compound per well at a concentration of 133 μM. The compound concentration is higher than those of the standard HTS libraries because fragments are generally weaker binders than their higher molecular weight counterparts. Activity was defined as >30–60% inhibition (depending upon the robustness of the assay) at the screening concentration. The number of fragment hits varied significantly between the targets and ranged from 12 to 1041 (see Table 2).

(d) Similarity Coefficients Compared for Performance Prediction and as a Benchmark of Virtual Fragment Linking. Virtual fragment linking attempts to generalize from fragment-based activity data to activities of larger molecules. The assumption regarding performance of this generalization would be that the better the fragments in the library describe the HTS molecule set (the "more similar" they are to each other), the better this generalization works.[22] In order to establish the relationship between similarity of fragment and full HTS data sets on the one hand and performance of predictions on the other hand, we investigated several similarity coefficients that were all used on ECFP4 fingerprints (as the models themselves).

The Tversky similarity coefficient[23] was calculated as shown in eq 1.

$$S(\text{Tversky})_{A,B} = \frac{c}{\alpha(a-c)+\beta(b-c)+c} \qquad (1)$$

Here, "*a*" represents the number of features present only in molecule A (and not in molecule B), "*b*" is the number of

Table 1. WOMBAT Data Sets Used in the Current Study[a]

target	target_fullname	family	no. compds submicromolar	no.compds double-digit MW LT 250	ROC score	ROC rating
5α-R1	5α-R1, 3-oxo-5-α-steroid 4-dehydrogenase 1	steroid 5-α-reductase	201	11	0.927	accuracy 0.927: excellent
5α-R2	5α-R2, 3-oxo-5-α-steroid 4-dehydrogenase 1	steroid 5-α-reductase	168	4	0.732	accuracy 0.732: fair
5-HT1A	5-HT1A, 5-hydroxytryptamine 1A receptor; serotonergic receptor	GPCR	21	4	0.838	accuracy 0.838: good
5-HTT	5-HTT, sodium-dependent serotonin transporter		176	7	0.703	accuracy 0.703: fair
5-LOX	5-LOX, arachidonate 5-lipoxygenase	lipoxygenase, dioxygenase	470	59	0.508	accuracy 0.508: fail
ACAT	ACAT, acylCoA:cholesterol O-acyltransferase	membrane-bound acyltransferase	34	5	0.540	accuracy 0.540: fail
AChE	AChE, acetylcholinesterase	GPCR	527	32	0.921	accuracy 0.921: excellent
AGAT	AGAT, methylated-DNA-protein-cysteine methyltransferase; O6-methylguanine-DNA methyltransferase	MGMT family	45	5	1.000	accuracy 1.000: excellent
ALK-5	ALK-5, activin receptor-like kinase 5; transforming growth factor-β type I receptor	serine/threonine-protein kinase, transforming growth factor-β receptor; transferase	102	3	1.000	accuracy 1.000: excellent
ALR	ALR, aldose reductase	aldo/keto reductase, oxidoreductase	181	8	0.893	accuracy 0.893: good
aromatase	aromatase, estrogen synthetase; cytochrome P450 19A1	cytochrome P450, oxidoreductase	257	80	0.938	accuracy 0.938: excellent
BChE	BChE, butyrylcholinesterase	GPCR	327	5	0.590	accuracy 0.590: fail
CA-II	CA-II, carbonic anhydrase I	eukaryotic-type carbonic anhydrase, lyase	231	5	0.945	accuracy 0.945: excellent
caspase-3	caspase-3, cysteine protease CPP32; apopain	peptidase C14, cysteine protease; hydrolase	146	3	0.798	accuracy 0.798: fair
cathepsin B	cathepsin B, APP secretase	peptidase C1, cysteine protease	97	7	0.967	accuracy 0.967: excellent
cathepsin L	cathepsin L, major excreted protein	peptidase C1, cysteine protease	92	3	0.737	accuracy 0.737: fair
CDK1/cyclin B	CDK1/cyclin B, cyclin-dependent kinase 1	serine/threonine-protein kinase, transferase	90	21	0.500	accuracy 0.500: fail
CDK2/cyclin A	CDK2/cyclin A, cyclin-dependent kinase 2	serine/threonine-protein kinase, transferase	258	9	0.500	accuracy 0.500: fail
CDK4	CDK4, cyclin-dependent kinase 4	serine/threonine-protein kinase, transferase	35	3	0.972	accuracy 0.972: excellent
COX-1	COX-1, prostaglandin H2 synthase 1; constitutive cyclooxygenase	prostaglandin G/H synthase, oxidoreductase; peroxidase; dioxygenase	150	8	0.536	accuracy 0.536: fail
COX-2	COX-2, prostaglandin H2 synthase 2; inducible cyclooxygenase	prostaglandin G/H synthase, oxidoreductase; peroxidase; dioxygenase	837	15	0.514	accuracy 0.514: fail
c-Raf	c-Raf, RAF proto-oncogene serine/threonine-protein kinase	serine/threonine-protein kinase, transferase	79	4	0.552	accuracy 0.552: fail
DAT	DAT, sodium-dependent dopamine transporter	sodium neurotransmitter symporter	195	4	0.820	accuracy 0.820: good
DHODHase	DHODHase, dihydroorotate oxidase	dihydroorotate dehydrogenase, oxidoreductase	35	4	0.564	accuracy 0.564: fail
DNA-PK	DNA-PK, DNA-dependent protein kinase	nuclear serine/threonine protein kinase, phosphatidylinositol 3-kinase; PIKK	50	7	1.000	accuracy 1.000: excellent
DPP II	DPP II, dipeptidyl peptidase II	peptidase S28, serine protease	74	35	0.999	accuracy 0.999: excellent
DPP IV	DPP IV, dipeptidyl peptidase IV	peptidase S28, serine protease	175	27	0.996	accuracy 0.996: excellent
DSPase	DSPase, dual specificity phosphatase Cdc25A	protein-tyrosine phosphatase, hydrolase	19	5	0.714	accuracy 0.714: fair
EGFR	EGFR, epidermal growth factor receptor	tyrosine-protein kinase, transferase	957	28	0.934	accuracy 0.934: excellent
eNOS	eNOS, nitric oxide synthase, endothelial; constitutive NOS	NOS, oxidoreductase	50	84	0.559	accuracy 0.559: fail
ERα	ERα, estrogen receptor	nuclear hormone receptor	416	54	0.861	accuracy 0.861: good
ERβ	ERβ, estrogen receptor β	nuclear hormone receptor	452	31	0.928	accuracy 0.928: excellent
E-selectin	E-selectin, leukocyte-endothelial cell adhesion molecule 2; endothelial leukocyte adhesion molecule 1; ELAM-1; CD62E antigen; LECAM1 2	selectin/LECAM	108	3	0.942	accuracy 0.942: excellent
FGFR	FGFR, fibroblast growth factor receptor 1	tyrosine-protein kinase, transferase	118	13	0.516	accuracy 0.516: fail
GAT1	GAT1, sodium- and chloride-dependent GABA transporter 1	sodium neurotransmitter symporter	3	4	1.000	accuracy 1.000: excellent

Table 1. Continued

target	target_fullname	family	no. compds submicromolar	no.compds double-digit MW LT 250	ROC score	ROC rating
H1	H1, histamine H1 receptor	GPCR	40	5	0.654	accuracy 0.654: poor
HLE	HLE, neutrophil elastase; leukocyte elastase	peptidase S1, serine protease	81	3	0.744	accuracy 0.744: fair
IKK	IKK, inhibitor of nuclear factor κ B kinase	serine/threonine-protein kinase, transferase	12	9	1.000	accuracy 1.000: excellent
IL-1β	IL-1β, interleukin-1 β; catabolin	cytokine	42	6	0.852	accuracy 0.852: good
iNOS	iNOS, nitric-oxide synthase, inducible	NOS, oxidoreductase	107	116	0.888	accuracy 0.888: good
L-CA	L-CA, leukocyte common antigen precursor; CD45 antigen	protein-tyrosine phosphatase, hydrolase	42	15	0.937	accuracy 0.937: excellent
Lck	Lck, proto-oncogene tyrosine-protein kinase Lck	tyrosine-protein kinase, transferase	229	4	0.614	accuracy 0.614: poor
m1	m1, muscarinic acetylcholine receptor M1	GPCR	71	6	0.837	accuracy 0.837: good
m2	m2, muscarinic acetylcholine receptor M2	GPCR	44	5	0.977	accuracy 0.977: excellent
m3	m3, muscarinic acetylcholine receptor M3	GPCR	37	5	0.987	accuracy 0.987: excellent
m4	m4, muscarinic acetylcholine receptor M4	GPCR	35	5	0.988	accuracy 0.988: excellent
mGluR1	mGluR1, metabotropic glutamate receptor 1	GPCR	80	4	0.593	accuracy 0.593: fail
mGluR2	mGluR2, metabotropic glutamate receptor 2	GPCR	16	3	0.993	accuracy 0.993: excellent
mGluR5	mGluR5, metabotropic glutamate receptor 5	flavin monoamine oxidase, flavin monoamine oxidase family	59	10	0.879	accuracy 0.879: good
MMP-1	MMP-1, fibroblast collagenase; matrix metalloprotease-1	peptidase M10A, hydrolase	514	5	0.803	accuracy 0.803: good
MMP-2	MMP-2, gelatinase A; matrix metalloprotease-2	peptidase M10A, hydrolase	423	10	0.796	accuracy 0.796: fair
MMP-3	MMP-3, matrix metalloprotease-3; stromelysin 1	peptidase M10A, hydrolase	589	3	0.791	accuracy 0.791: fair
MMP-8	MMP-8, matrix metalloprotease-8; neutrophil collagenase	peptidase M10A, hydrolase	130	5	0.760	accuracy 0.760: fair
MMP-9	MMP-9, gelatinase B; matrix metalloprotease-9	peptidase M10A, hydrolase	580	3	0.795	accuracy 0.795: fair
muscarinic	muscarinic, muscarinic acetylcholine receptor	GPCR	51	14	0.969	accuracy 0.969: excellent
NAALADase	NAALADase, glutamate carboxypeptidase II; N-acetylated-α-linked acidic dipeptidase I	peptidase M28	20	11	0.999	accuracy 0.999: excellent
NET	NET, sodium-dependent norepinephrine transporter	sodium neurotransmitter symporter	111	5	0.830	accuracy 0.830: good
NF-κB	NF-κB, nuclear factor NF-κ-B	Rel/dorsal family	106	3	0.649	accuracy 0.649: poor
NHE-1	NHE-1, Na(+)/H(+) antiporter, amiloride-sensitive; Na(+)/H(+) exchanger 1; Na(+)/H(+) antiporter, amiloride-sensitive	Na(+)/H(+) exchanger	65	12	0.970	accuracy 0.970: excellent
nNOS	nNOS, neuronal nitric oxide synthase; constitutive NOS; NOS, type I	NOS, oxidoreductase	81	63	0.585	accuracy 0.585: fail
PARP	PARP, poly(ADP-ribose) polymerase-1; NAD(+) ADP-ribosyltransferase; poly(ADP-ribose) synthetase	glycosyltransferase	77	8	0.976	accuracy 0.976: excellent
PARP1	PARP1, poly(ADP-ribose) polymerase-1; NAD(+) ADP-ribosyltransferase; poly(ADP-ribose) synthetase	glycosyltransferase	101	7	0.971	accuracy 0.971: excellent
PDE3	PDE3, cGMP-inhibited PDE	cyclic nucleotide phosphodiesterase, hydrolase	250	3	0.930	accuracy 0.930: excellent
PDE4	PDE4, cAMP-specific PDE	cyclic nucleotide phosphodiesterase, hydrolase	466	13	0.784	accuracy 0.784: fair
PDGFR	PDGFR, platelet derived growth factor receptor	hormone/growth factor	248	39	0.587	accuracy 0.587: fail
PNP	PNP, purine nucleoside phosphorylase	PNP/MTAP phosphorylase, transferase	15	8	1.000	accuracy 1.000: excellent
PTP-1B	PTP-1B, protein-tyrosine phosphatase 1B	protein-tyrosine phosphatase, hydrolase	126	15	0.753	accuracy 0.753: fair

Table 1. Continued

target	target_fullname	family	no. compds submicromolar	no.compds double-digit MW LT 250	ROC score	ROC rating
sEH	sEH, soluble epoxide hydrolase; cytosolic epoxide hydrolase	AB hydrolase	115	56	1.000	accuracy 1.000: excellent
StSase	StSase, steroid sulfatase; estrone sulfatase	sulfatase, hydrolase	93	4	0.909	accuracy 0.909: excellent
TNFα	TNFα, tumor necrosis factor-α; cachectin		173	3	0.527	accuracy 0.527: fail
TPase	TPase, thymidine phosphorylase	thymidine/pyrimidine-nucleoside phosphorylase	5	3	1.000	accuracy 1.000: excellent
TSase	TSase, thymidylate synthase	thymidylate synthase, transferase; methyltransferase	70	30	0.924	accuracy 0.924: excellent
TXA2 synthase	TXA2 synthase, thromboxane A2 synthase	cytochrome P450, monooxygenase	317	22	0.869	accuracy 0.869: good
VCAM-1	VCAM-1, vascular cell adhesion molecule-1		32	10	0.982	accuracy 0.982: excellent
VEGFR-2	VEGFR-2, vascular endothelial growth factor receptor 2	tyrosine-protein kinase, transferase	728	6	0.815	accuracy 0.815: good
			13557	1157		

[a] For each of the 75 data sets, the target name, target family, number of fragments and compounds used, and the quality of the generated model are given.

Table 2. FBS In-House Data Sets Selected for This Study[a]

assay no.	target class	assay type	no. of active fragments in model	no. of active compds from HTS library confirmed with $IC_{50} < 10\ \mu M$	
				total	captured by VFL
1	GPCR	cell based	241	604	406 (67.2%)
2	kinase 1	enzymatic	107	703	371 (52.8%)
3	kinase 2	enzymatic	1041	1377	675 (49.0%)
4	kinase 3	enzymatic	850	567	157 (27.7%)
5	estrogen receptor	cell based	12	52	7 (13.5%)
6	metalloproteinase	enzymatic	104	115	10 (8.7%)
7	channel	cell based	545	281	13 (4.6%)

[a] For the GPCR and the kinases, good models were obtained, but this was not the case for the estrogen receptor, the metalloproteinase, and the ion channel.

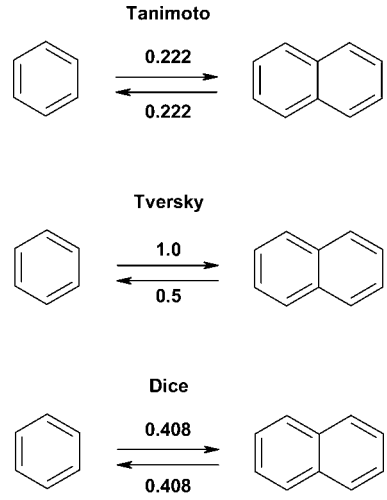

Figure 4. Comparison of Tanimoto, Dice, and Tversky similarity coefficients for benzene and naphthalene. The similarity coefficients are shown near the arrows. The Tversky coefficient focuses on the substructural relationship of the library compound to the query structure. In this case, benzene as the query structure would completely be contained in naphthalene as was the library structure, thus assigning this molecular pair a Tversky similarity of 1.

features present only in molecule B (and not in molecule A), and "*c*" is the number of features in common between molecules A and B.

Values of $\alpha = 1$ and $\beta = 0$ were used, and the behavior of these values is illustrated in Figure 4. Since $\beta = 0$, the value of *b*, the number of features only present in molecule B, disappears from the equation. This means that even if there are features only present in molecule B, it does not influence the similarity between the structures at all; the coefficient establishes similarity as a measure of how well molecule A is contained *within* molecule B. If molecule A is a full substructure of molecule B, the similarity of molecules A and B using this measure would always be equal to 1, no matter what additional appendages molecule B might have. Thus, the Tversky similarity between benzene and naphthalene is 1, since naphthalene completely contains benzene as a substructure (and additional functionalities do not influence the similarity value). The reason to use this asymmetrical similarity measure as a potential predictor of performance was that we provide the model with fragment-based screening data that consist in every case of smaller molecules than the test set, so the maximum similarity (corresponding to a value of 1) could be achieved in the case of total substructural matches and not in the case of structural identity (which would not be achievable in this case).

The first application of the Tversky similarity coefficient, based on ECFP4 fingerprints, is thus to correlate (or predict) the performance of the fragment-based model, based on the similarity of the fragment and the HTS library. The second application of the Tversky index is its use as a benchmark for virtual fragment linking. By identification of molecules in the HTS library that are the most similar to the fragments found to be active, those compounds could also be suggested as actives straightaway. We hoped to outperform simple similarity searching by using VFL, since VFL is based on Bayes models that use information from *multiple* fragments in the model, while similarity coefficients are not able to "pool" features and make generalizations to molecules containing new mixtures of fragments. As an alternative to the Tversky coefficient, we also employed the symmetrical Tanimoto similarity coefficient,[24]

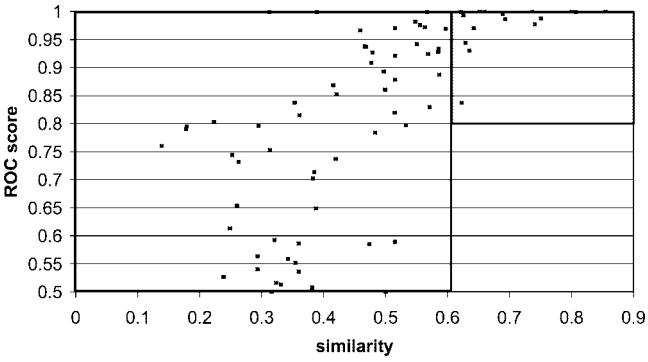

Figure 5. Quality of the WOMBAT data sets predictions (measured as ROC values) as a function of mean nearest neighbor Tversky similarity between fragment and HTS data sets. If the mean similarity between both data sets reaches a value of about 0.6, prioritization of the full library based on fragment screening data can be consistently performed with values of ROC > 0.8. Thus, the chemical space coverage of the fragment library is important for fragment hit generation and for generalizability of the model to small molecules.

which corresponds to eq 1 with $\alpha = \beta = 1$, as well as the Dice coefficient (where $\alpha = \beta = {}^1/_2$).

(e) Model Performance Measure for WOMBAT Models: ROC Score. The receiver operating characteristic (ROC) score is a commonly used measure of model performance for binary classification,[25] and it was used in this work as a performance measure on the WOMBAT data set. It is defined by selectivity along the *Y* axis and by 1-specificity along the *X* axis. An ROC score of 1 achieves perfect classification (no false positives or negatives), while an ROC score of 0.5 indicates a random model. This ROC score effectively describes how well our fragment-based activity model is able to classify HTS compounds for that particular activity. It should be kept in mind that ROC scores provide an overall performance measure of the model, although in practice certain areas of the model are often considered to be particularly relevant compared to other areas (e.g., the top 1% or top 5% of compounds suggested to be screened by a virtual screening model).

(f) Model Performance Measure for In-House Models: Retrieval of Actives. The performance measures and workflow on the internal data sets were slightly different from those based on the WOMBAT data mainly because of the different kind of data at hand. For the in-house FBS data, all compounds were screened at concentrations of 133 μM, and an inhibition of >30–60%, depending on robustness of the assay, was defined as being active. On the basis of this fragment-based model, the fraction of active HTS compounds in the top 5% of the ranked full HTS library was calculated. Prospectively, the idea is to use FBS data to prioritize the full HTS library, thus decreasing overall screening expenditure, and 5% of our full HTS library is approximately what could be cherry-picked in one day using robots.

3.Results and Discussion

(a) Virtual Fragment Linking on WOMBAT Data Sets. In order to get an idea of the performance of virtual fragment linking across a wide variety of targets and activity classes, we first employed fragment-based models for 75 WOMBAT activity classes. The names of the activity classes along with target classification and details about the data sets are given in Table 1. When creating an activity model and scoring the HTS library for that activity class, we calculated an ROC score as described in the Methods section. The success of the VFL algorithm in the form of ROC scores is depicted in Figure 5. Every data point in Figure 5 corresponds to the ROC score of a particular model (for details, see Table 1) plotted along the *Y* axis. The *X* axis on the other hand is defined by the mean nearest neighbor Tversky similarity, per activity class, between the fragment data set used for training and the HTS data set used as a test set.

We see that for 45 out of the 75 targets (60%) the accuracy of the fragment-based models was good or excellent (ROC > 0.8; model performance classification according to rules implemented in Pipeline Pilot), for 12 targets (16%) it was fair (0.8 > ROC > 0.7), while for the 18 remaining targets (24%) it was poor (ROC < 0.7). Figure 5 also shows that the ROC scores are correlated to the mean nearest neighbor Tversky similarity between the fragments and the HTS library compounds found to be active in each class. High Tversky similarity coefficients (>0.6) are correlated with good or excellent performance of VFL (ROC > 0.8) in every case. This means that a fragment library that describes the substructures contained in the HTS library rather well can be used to make predictions about it. The reverse is not true. Small mean nearest neighbor similarities between fragments and the HTS library can lead to good or bad performance of the model, but this behavior cannot be predicted in any way. We can conclude from this part of the study that given a library of small-molecule binders with MW < 250 and IC_{50} values in the micromolar range, we can predict nanomolar activity of larger compounds if, as an empirical rule, the mean nearest neighbor Tversky similarity between fragment and HTS library is larger than 0.7. Still, when it comes to retrieving active compounds, virtual fragment linking was overall outperforming the Tversky index probably because of its ability to link individual fragments to generalize to larger, more potent compounds from the full HTS library.

(b) Feature Analysis on the WOMBAT Data Set: From Low Potency Fragments to Potent Compounds. To further demonstrate the ability of virtual fragment linking to capture potent compounds from weak actives, we selected two additional activity classes from WOMBAT with the aim to interpret and understand behavior of the method. For both of the activity classes structural information is available in the literature as an X-ray structure or at least as a docking hypothesis. The first activity class was an enzyme of the cytochrome P450 superfamily, aromatase, which aromatizes androgens producing estrogens. Aromatase inhibitors are used to treat breast cancer following relapse of tamoxifen therapy.[26,27] The IC_{50} distribution for the selected compounds in this activity class is shown in the lower part of Figure 2, and the fragment training set was defined by MW < 250 and potency in the micromolar range. The process by which virtual fragment linking captures potent compounds is illustrated in Figure 6; IC_{50} values in this case range between 69 and 280 nM. Ten fragments from the fragment training set are displayed in the upper part of Figure 6, followed by 15 examples of important features in the fragments. We see that the triazole and imidazole groups, present in compounds **5** and **6**,[28] were identified by the VFL algorithm as beneficial to activity. Literature research confirms that indeed those inhibitors bind to the active site through coordination of a heterocyclic nitrogen lone pair to the iron cation.[29] This is equally true for the pyridine ring in compounds **7** and **8**,[29] showing that our fragment-based activity model consists of submodels that try to capture bioisosteric functionalities. The benzylic methoxy group in all four compounds was also identified by VFL as important. The methoxy substituent may act as a hydrogen bond acceptor depending on the binding mode of the compound, which may differ among the binders.[29] An appealing feature of VFL is that it is able to combine features from multiple

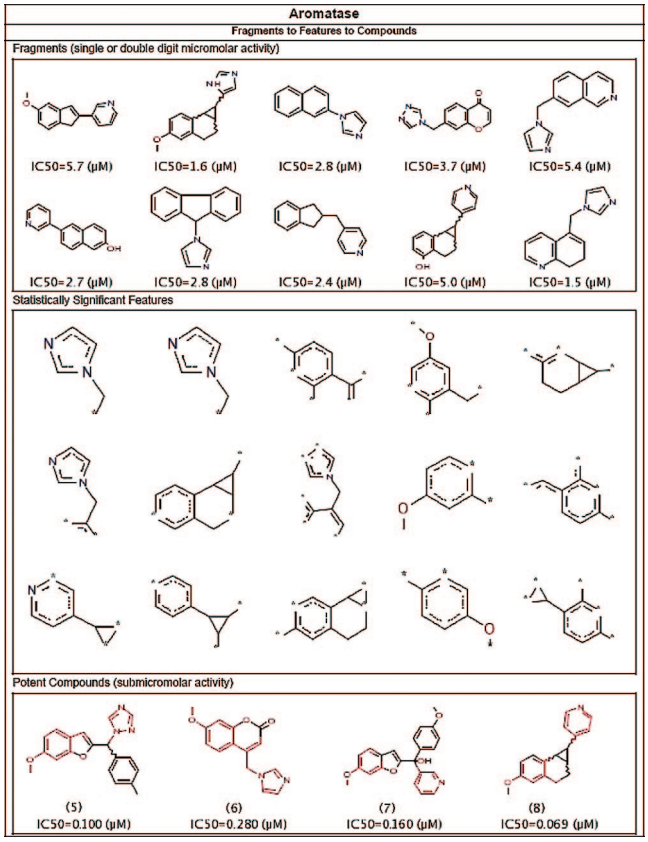

Figure 6. Analysis of the fragments active against aromatase, features contained within the fragments, and HTS compounds that contain features previously found in the fragment set (marked in red).

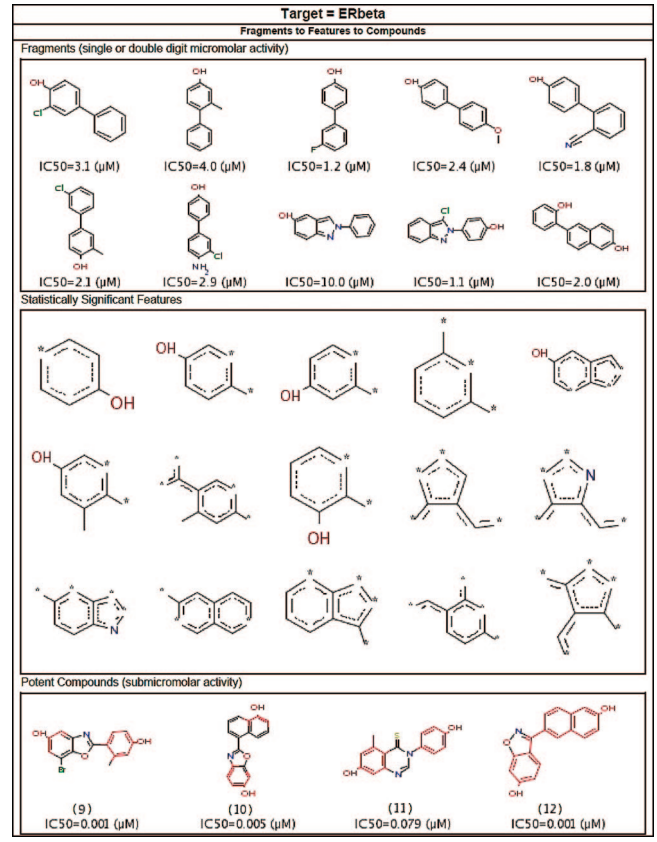

Figure 7. Analysis of the fragments active against the estrogen β receptor, features contained within the fragments, and HTS compounds that contain features previously found in the fragment set (marked in red).

fragments to suggest new, more potent compounds: For example, compound **8** with $IC_{50} = 69$ nM combined the features stemming from a fragment with $IC_{50} = 5$ μM with a benzylic methoxy function present in other micromolar binders, increasing potency by 2 orders of magnitude. This corroborates the computational ability of our method to link fragments to arrive at more potent hits.

The second example, estrogen receptor β (ERβ) is overexpressed in most cases of breast cancer, rendering it a target with great therapeutic potential.[30] Figure 7 depicts the identification of compounds **9**–**12** with an IC_{50} range between 1 and 79 nM.[31] The aromatic groups and specifically the two phenol rings were identified by VFL as the most important features, as shown in the center of the figure. This finding is indeed supported by the literature.[31] Since for ERβ cocrystals were available in the PDB with compounds **10** and **12**, we followed up with an analysis of the features identified by us as being important and those present in the crystal structures (the PDB codes are 1u3s and 1u3r, respectively[31]). As shown in Figure 8, the crystal structures demonstrate how phenol motifs bind in the ERβ pocket. In both cases, hydrogen bonds and charge interactions with Glu305 and Arg346 on the one hand, and with His475 on the other hand, are responsible for binding, with the central part of the system mainly being responsible for keeping the oxygens at an appropriate distance from each other for binding. Also in this case sensible agreement between features selected from fragment-based screening data and the crystal structure of ligand-target cocrystals can be established.

(c) Virtual Fragment Linking on In-House FBS Data Sets. The WOMBAT data sets demonstrated how VFL employed on low micromolar fragments captured the significant chemical features and linked them to more potent compounds. However, the number of very low affinity fragments in the WOMBAT database was insufficient because most of the assays used for the targets in this database were not designed to detect compounds with $IC_{50} < 30$ μM. Low affinity FBS hits are interesting because most of the FBS hits that one obtains using NMR or by screening at a very high concentration are in the low affinity range ($K_d > 50$ μM). Therefore, we further challenged the method by selecting in-house fragment hits that were very weak binders and in certain situations even false positives. The performance measures and workflow on the internal data sets were slightly different from those based on the WOMBAT data, mainly because of the different kind of data at hand. For the in-house FBS data, all compounds were screened at 133 μM, and an inhibition of >30–60%, depending on robustness of the assay, was defined as being active. On the basis of this fragment-based model, the fraction of active HTS compounds in the top 5% of the ranked library was calculated (instead of the ROC models used on the WOMBAT data set).

Figure 9 depicts the fraction of compounds confirmed with $IC_{50} < 10$ μM that were captured by the top 5% of the ranked library for each of the seven targets. For the majority of targets, VFL captured between 28% and 67% of the hits that were identified by screening the full collection. For the GPCR and the three kinases on average 49.2% of all actives were retrieved in the top 5% of the ranked HTS database, which corresponds to a 10-fold enrichment. Virtual fragment linking was found to be consistently superior to similarity searching (which is not able to generate models based on features from multiple fragments). This is true in all cases except for the ion channel target. In this case Tversky similarity searching outperformed VFL (8.2% vs 4.6%). We can conclude that on this particular

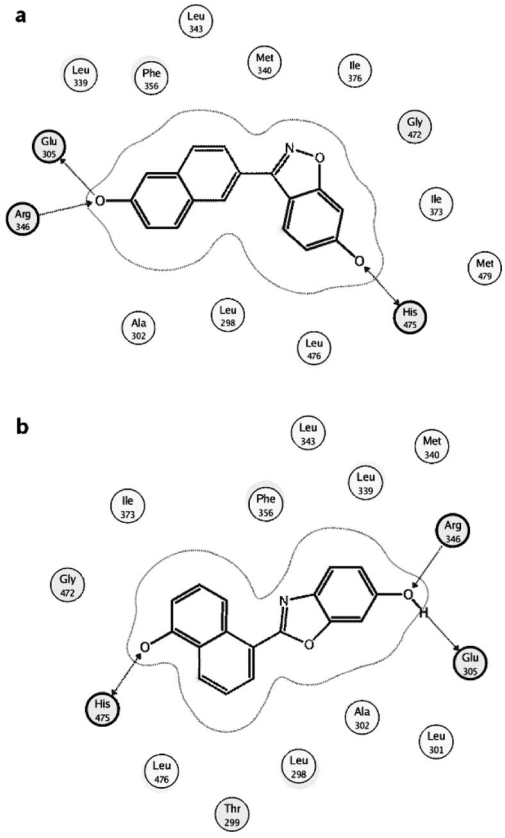

Figure 8. ERβ binding site with bound ligands: (a) compound **12** as found in 1u3s.pdb and (b) compound **10** in 1u3r.pdb. The attractive features captured by VFL are highlighted by bold circles around the amino acids. The binding occurs between one of the phenol rings and Arg 346 and Glu 205. Also, His 475 forms a hydrogen bond to the opposing phenol ring.

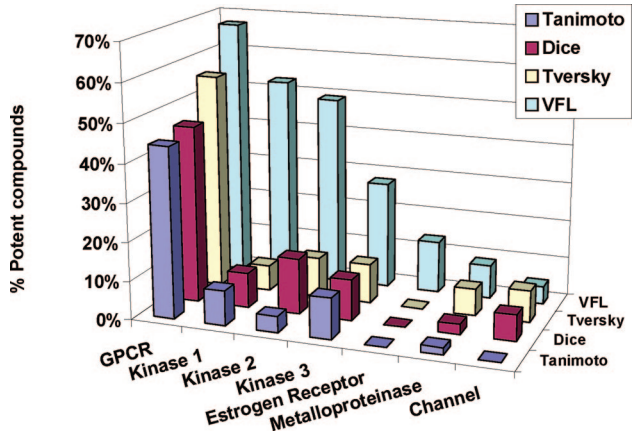

Figure 9. Percentage of potent compounds captured at the top 5% (50 000 compounds) of the ranked library. Compared are virtual fragment linking (VFL) and simple similarity searching using Tversky, Tanimoto, and Dice coefficients between the fragment and the full HTS library.

target neither similarity searching nor virtual fragment linking achieved good results. One likely reason is that the fragment library does not cover active space well enough to be predictive for the active molecules from the HTS set. Figure 9 also shows three different metrics of similarity: Tanimoto, Tversky, and Dice coefficients. Because of the inconsistencies among the three metrics of similarity, it was difficult to conclude which one was preferable. The GPCR and the three kinases are successful examples of applying VFL in lead finding though, since many

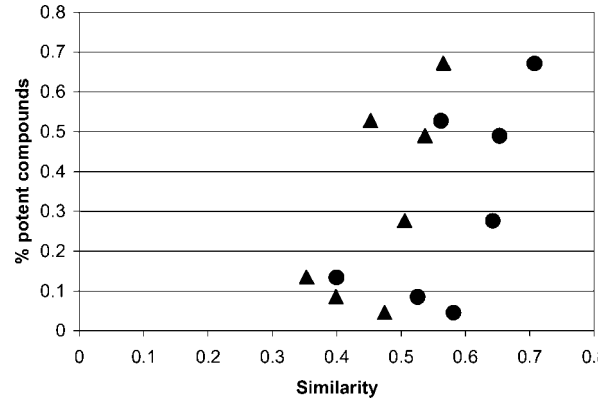

Figure 10. Mean nearest neighbor Tversky (circles) and Dice (triangles) coefficients between the fragment library and the validated compounds with $IC_{50} < 10\mu M$ for each of the seven targets in the in-house library. Higher similarity coefficients are related to a higher percentage of potent compounds captured by the "virtual fragment linking" algorithm.

more active compounds are retrieved than by any similarity searching coefficient.

As in the case of the WOMBAT data set, we were trying to find predictors of the performance of VFL in order to judge its applicability prospectively. Figure 10 depicts the mean nearest neighbor similarity between the fragment library and the HTS actives for each of the seven targets using Tversky and Dice coefficients. High average Tversky similarity (>0.6) or a high average Dice coefficient (>0.5) is correlated with better predictions. These results are similar compared to the results for WOMBAT (Figure 5) where a Tversky cutoff of >0.7 was established for consistently reliable models.

Thus, as a general trend, the 2D similarity between the fragments that were screened and the fraction of potent compounds in full HTS chemical space that can be extrapolated to is extremely important for VFL. One needs fragments in the FBS library that resemble potential HTS hits in the full library. This has crucial ramifications in terms of fragment library design. Kinases and GPCRs were heavily studied targets in the biopharmaceutical industry in recent years. As a result, the fragment library employed in this study was rich in kinase- and GPCR-related fragments, leading to successful predictions for HTS actives in those activity classes. In contrast, when the average mean nearest neighbor similarity between fragment and HTS library was low, the predictive value of the fragment-based model was diminished. This followed with the commonly held conception that if an active molecule's neighbors were similar, then they too may be active.[22,32]

An important direction for the future is an extension of the current fragment library to cover more chemotypes and thus a wider range of targets. For example, only 12 fragment hits were identified for the estrogen receptor compared to 107, 850, and 1041 hits for the three kinases, respectively. We postulate here that adding additional fragments, in particular those showing high Tversky similarity to the HTS hits for those targets, will increase the likelihood of success at a smaller cost (number of compounds screened) than when using the full HTS deck. For novel targets where no HTS hits have been found yet, a family based approach can be pursued. In the example above, fragments that should improve predictivity of the fragment model for the estrogen β receptor are likely also to be of value for other nuclear hormone receptors, and similarly the idea goes for other target families.

To summarize, it seems that the prerequisite for virtual fragment linking to work well is a high mean nearest neighbor

similarity between fragment and HTS libraries. A Tversky similarity >0.6–0.7 is suggested in our case for both WOMBAT and in-house data sets. This was the case in the current study for heavily pursued targets such as GPCRs and kinases; therefore, good models were obtained. However, this was not true for the estrogen receptor, the metalloproteinase, and the ion channel. Either diversity-based or family fragment-based enhancement of our fragment library would be possible approaches to improve the odds of being successful in FBS, and we are currently following up both of those paths.

4. Conclusions

In this work we explored the possibilities of using fragment-based screening data to prioritize compounds from a full HTS campaign, a method we called "virtual fragment linking". The aim of the work was to decrease screening expenditure by prioritizing HTS libraries using fragment-based screening data and to explore to what extent this can be done successfully. For both literature and internal data, results were largely consistent. For generating predictive models from hits in fragment-based screens, the fragment library needs to contain fragments relevant to the target. Retrospectively, this measure of "relevance to the target" was established as a mean nearest neighbor Tversky similarity value between fragment and full library above 0.6 and 0.7 for in-house and literature data, respectively (based on ECFP4 fingerprints). This was true for 75 targets from WOMBAT, as well as for 7 targets screened internally. Large deviations in mean nearest neighbor similarity between fragment and full library could be explained by the nature of the target. For a GPCR and a set of kinases, the fragment libraries were equipped rather well, leading to favorable results. In those four cases on average 49.2% of all actives were retrieved in the top 5% of the ranked HTS database, which corresponds to a 10-fold enrichment. For the estrogen receptor, a metalloproteinase, and an ion channel this was not the case. This lets us conclude that proper coverage of chemical space by the fragment library is crucial. If one attempts to find hits in fragment-based screening, relevant fragments need to be in the library in the first run. Eliminating target bias would also be beneficial with respect to FBS hit rates as well as model predictivity for less usual targets.

In this study FBS was done in biochemical and cell based assays. This type of data may be contaminated with false positives that might skew the identification of features. It would be of value to compare this screening strategy with "classical" FBS using NMR (or other biophysical methods). Methods such as NMR are likely to perform better because hit lists may contain fewer false positives.

In comparing the value of virtual fragment linking to nearest neighbor similarity searching using the Tversky, Dice, and Tanimoto coefficient, we see that virtual fragment linking outperforms similarity searching on the data sets used here. For example cases, we were able to trace this behavior back to the ability of virtual fragment linking to combine features (and thus fragments) in the activity model, thus being able to generalize to novel molecules.

References

(1) Burbaum, J. J.; Sigal, N. H. New technologies for high-throughput screening. *Curr. Opin. Chem. Biol.* **1997**, *1*, 72–78.
(2) Bohacek, R. S.; McMartin, C.; Guida, W. C. The art and practice of structure-based drug design: a molecular modeling perspective. *Med. Res. Rev.* **1996**, *16*, 3–50.
(3) Fink, T.; Bruggesser, H.; Reymond, J. L. Virtual exploration of the small-molecule chemical universe below 160 daltons. *Angew. Chem., Int. Ed.* **2005**, *44*, 1504–1508.
(4) Lipinski, C.; Hopkins, A. Navigating chemical space for biology and medicine. *Nature* **2004**, *432*, 855–861.
(5) Zartler, E. R.; Shapiro, M. J. Fragonomics: fragment-based drug discovery. *Curr. Opin. Chem. Biol.* **2005**, *9*, 366–370.
(6) Rees, D. C.; Congreve, M.; Murray, C. W.; Carr, R. Fragment-based lead discovery. *Nat. Rev. Drug Discovery* **2004**, *3*, 660–672.
(7) Erlanson, D. A.; McDowell, R. S.; O'Brien, T. Fragment-based drug discovery. *J. Med. Chem.* **2004**, *47*, 3463–3482.
(8) Lesuisse, D.; Lange, G.; Deprez, P.; Benard, D.; Schoot, B.; Delettre, G.; Marquette, J. P.; Broto, P.; Jean-Baptiste, V.; Bichet, P.; Sarubbi, E.; Mandine, E. SAR and X-ray. A new approach combining fragment-based screening and rational drug design: application to the discovery of nanomolar inhibitors of Src SH2. *J. Med. Chem.* **2002**, *45*, 2379–2387.
(9) Hartshorn, M. J.; Murray, C. W.; Cleasby, A.; Frederickson, M.; Tickle, I. J.; Jhoti, H. Fragment-based lead discovery using X-ray crystallography. *J. Med. Chem.* **2005**, *48*, 403–413.
(10) Shuker, S. B.; Hajduk, P. J.; Meadows, R. P.; Fesik, S. W. Discovering high-affinity ligands for proteins: SAR by NMR. *Science* **1996**, *274*, 1531–1534.
(11) Mauser, H.; Stahl, M. Chemical fragment spaces for de novo design. *J. Chem. Inf. Model.* **2007**, *47*, 318–324.
(12) Connolly, S.; Aberg, A.; Arvai, A.; Beaton, H. G.; Cheshire, D. R.; Cook, A. R.; Cooper, S.; Cox, D.; Hamley, P.; Mallinder, P.; Millichip, I.; Nicholls, D. J.; Rosenfeld, R. J.; St-Gallay, S. A.; Tainer, J.; Tinker, A. C.; Wallace, A. V. 2-Aminopyridines as highly selective inducible nitric oxide synthase inhibitors. Differential binding modes dependent on nitrogen substitution. *J. Med. Chem.* **2004**, *47*, 3320–3323.
(13) Hert, J.; Willett, P.; Wilton, D. J.; Acklin, P.; Azzaoui, K.; Jacoby, E.; Schuffenhauer, A. Comparison of topological descriptors for similarity-based virtual screening using multiple bioactive reference structures. *Org. Biomol. Chem.* **2004**, *2*, 3256–3266.
(14) Glick, M.; Jenkins, J. L.; Nettles, J. H.; Hitchings, H.; Davies, J. W. Enrichment of high-throughput screening data with increasing levels of noise using support vector machines, recursive partitioning, and Laplacian-modified naive Bayesian classifiers. *J. Chem. Inf. Model.* **2006**, *46*, 193–200.
(15) Bender, A.; Mussa, H. Y.; Glen, R. C.; Reiling, S. Similarity searching of chemical databases using atom environment descriptors (MOLPRINT 2D): evaluation of performance. *J. Chem. Inf. Comput. Sci.* **2004**, *44*, 1708–1718.
(16) Glen, R. C.; Bender, A.; Arnby, C. H.; Carlsson, L.; Boyer, S.; Smith, J. Circular fingerprints: flexible molecular descriptors with applications from physical chemistry to ADME. *IDrugs* **2006**, *9*, 199–204.
(17) *SciTegic Pipeline Pilot*, version 6.0; Accelrys: San Diego, CA; http://www.accelrys.com/.
(18) Nidhi; Glick, M.; Davies, J. W.; Jenkins, J. L. Prediction of biological targets for compounds using multiple-category bayesian models trained on chemogenomics databases. *J. Chem. Inf. Model.* **2006**, *46*, 1124–1133.
(19) Xia, X. Y.; Maliski, E. G.; Gallant, P.; Rogers, D. Classification of kinase inhibitors using a Bayesian model. *J. Med. Chem.* **2004**, *47*, 4463–4470.
(20) Tinker, A. C.; Beaton, H. G.; Boughton-Smith, N.; Cook, T. R.; Cooper, S. L.; Fraser-Rae, L.; Hallam, K.; Hamley, P.; McInally, T.; Nicholls, D. J.; Pimm, A. D.; Wallace, A. V. 1,2-Dihydro-4-quinazolinamines: potent, highly selective inhibitors of inducible nitric oxide synthase which show antiinflammatory activity in vivo. *J. Med. Chem.* **2003**, *46*, 913–916.
(21) *World of Biomolecular Activity (WOMBAT)*; SunSet Molecular Discovery LLC: Santa Fe, NM; http://www.sunsetmolecular.com.
(22) Bender, A.; Glen, R. C. Molecular similarity: a key technique in molecular informatics. *Org. Biomol. Chem.* **2004**, *2*, 3204–3218.
(23) Tversky, A. Features of Similarity. *Psychol. Rev.* **1977**, *84*, 327–354.
(24) Jaccard, P. Étude comparative de la distribution florale dans une portion des Alpes et des Jura (Comparative study of the distribution in a floral portion of the Alps and the Jura). *Bull. Soc. Vaudoise Sci. Nat.* **1901**, *37*, 547–579.
(25) Triballeau, N.; Acher, F.; Brabet, I.; Pin, J. P.; Bertrand, H. O. Virtual screening workflow development guided by the "receiver operating characteristic" curve approach. Application to high-throughput docking on metabotropic glutamate receptor subtype 4. *J. Med. Chem.* **2005**, *48*, 2534–2547.
(26) Bruno, R. D.; Njar, V. C. O. Targeting cytochrome P450 enzymes: a new approach in anti-cancer drug development. *Bioorg. Med. Chem.* **2007**, *15*, 5047–5060.
(27) Persing, M.; Grosse, R. Current St. Gallen recommendations on primary therapy of early breast cancer. *Breast Care* **2007**, *2*, 137–140.
(28) Saberi, M. R.; Vinh, T. K.; Yee, S. W.; Griffiths, B. J. N.; Evans, P. J.; Simons, C. Potent CYP19 (aromatase) 1-[(benzofuran-2-yl)(phenylmethyl)pyridine, -imidazole, and -triazole inhibitors: synthesis and biological evaluation. *J. Med. Chem.* **2006**, *49*, 1016–1022.
(29) Leonetti, F.; Favia, A.; Rao, A.; Aliano, R.; Paluszcak, A.; Hartmann, R. W.; Carotti, A. Design, synthesis, and 3D QSAR of novel potent and selective aromatase inhibitors. *J. Med. Chem.* **2004**, *47*, 6803–6792.

(30) Gungor, T.; Chen, Y.; Golla, R.; Ma, Z. P.; Corte, J. R.; Northrop, J. P.; Bin, B.; Dickson, J. K.; Stouch, T.; Zhou, R.; Johnson, S. E.; Seethala, R.; Feyen, J. H. M. Synthesis and characterization of 3-arylquinazolinone and 3-arylquinazolinethione derivatives as selective estrogen receptor beta modulators. *J. Med. Chem.* **2006**, *49*, 2440–2455.

(31) Malamas, M. S.; Manas, E. S.; McDevitt, R. E.; Gunawan, I.; Xu, Z. B.; Collini, M. D.; Miller, C. P.; Dinh, T.; Henderson, R. A.; Keith, J. C.; Harris, H. A. Design and synthesis of aryl diphenolic azoles as potent and selective estrogen receptor-beta ligands. *J. Med. Chem.* **2004**, *47*, 5021–5040.

(32) Patterson, D. E.; Cramer, R. D.; Ferguson, A. M.; Clark, R. D.; Weinberger, L. E. Neighborhood behavior: a useful concept for validation of "molecular diversity" descriptors. *J. Med. Chem.* **1996**, *39*, 3049–3059.

JM701314U